





Itinerant ferromagnetism of a dipolar Fermi gas with Raman-induced spin-orbit couplingXue-Jing Feng , Xing-Dong Zhao *, Lu Qin, Ying-Ying Zhang, and Zunlue Zhu
*School of Physics, Henan Normal University, Xinxiang 453000, China*Hong-Juan Tian
*College of Computer and Information Engineering, Henan Normal University, Xinxiang 453007, China
and School of Physics, Henan Normal University, Xinxiang 453000, China*Lin Zhuang
*State Key Laboratory of Optoelectronic Materials and Technologies, School of Physics,
Sun Yat-Sen University, Guangzhou 510275, China*Wu-Ming Liu [†]
*Beijing National Laboratory for Condensed Matter Physics, Institute of Physics, Chinese Academy of Sciences, Beijing 100190, China
and Songshan Lake Material Laboratory, Dongguan, Guangdong 523808, China* (Received 14 December 2021; revised 18 March 2022; accepted 12 May 2022; published 31 May 2022)

We elucidate the itinerant ferromagnetism of a dipolar Fermi gas with a Raman-induced spin-orbit coupling by investigating the exotic phase diagrams. It is revealed that the dipolar interaction along with spin-orbit coupling can corroborate the formation of ferromagnetism and that the Raman coupling adversely eliminates the tendency to this ferromagnetism transition, which greatly transcends the general understanding of this subject with contact interaction only. We explore the ground states through the density and spin-flip distribution in momentum space. We calculate the transition temperatures well within the reach of an experimental system when altering the dipolar and spin-orbit-coupling strength, which paves a way to the further experimental realization.

DOI: [10.1103/PhysRevA.105.053312](https://doi.org/10.1103/PhysRevA.105.053312)**I. INTRODUCTION**

Itinerant ferromagnetism has been a subject of conspicuous interest in the history of physics. Early in the last century when dealing with the itinerant electron gas within the Hartree-Fock approximation, Bloch pointed out that a ferromagnetic state could occur below a critical density at which the long-range Coulomb potential began to prevail over the kinetic energy. Thereafter Stoner studied the ferromagnetic properties in transition metals and gave a theoretical explanation [1,2] in which he replaced the Coulomb interaction with a screening repulsive contact potential. Subsequently in *d*-electron metals, the tight-binding method was commonly used, including the single-band Hubbard model [3,4]. Unlike in a solid state system, a more rapidly developing quantum gas which is best known for its high tunability in both inner interactions and external magnetic or optical fields can provide a different experimental platform for and at the same time theoretically stimulate this intricate problem.

Experimental breakthrough came when Jo *et al.* reported the investigation of the ferromagnetism transition in the ⁶Li system [5]. Following that, however, was some theoretical dispute arguing that the experimental result was not

convincing enough because no magnetic domains were captured, and instead of the ferromagnetic state fermions might choose to be as interaction increased, a short-range correlation state could also be a candidate to reduce the interaction energy [6–8]. So further experimental explorations were carried out to verify the occurrence of the ferromagnetic state [9,10]. Meanwhile, many theoretical works made contributions to this subject. Beyond the mean-field approach, a second-order perturbation calculation [11] was done, which obtained a critical phase transition point at $k_F a_s \approx 1.054$, where k_F was the Fermi wave vector and a_s was the *s*-wave scattering length. Other nonperturbative theoretical methods [12–14] as well as quantum Monte Carlo simulations [15–18] were also performed. In fact, when we are studying the ferromagnetic instability of an ultracold Fermi gas, formation of molecules generated by three-body recombination [19,20] and the competing BCS pairing instability [21,22] shall be inevitably considered when this system undergoes a BEC-BCS crossover by tuning a_s through the Feshbach resonance. From another perspective, the occurrence of a ferromagnetic state can be seen as a spin-imbalanced circumstance [23] in which a Fermi polaron is an interesting issue [24–26]. It is also found in several works that the mass imbalance in Fermi mixtures of which the usual two-component Fermi gas may be viewed as an equal-mass limit can stabilize the ferromagnetism [24,27,28]. Other focuses on itinerant ferromagnetism are the explorations of dynamical properties in Fermi gas [29–34] as well as the nonequilibrium non-Hermitian effect [35].

*phyzhxd@gmail.com

[†]wmliu@iphy.ac.cn

However, most of the previous works on quantum gas were concentrating on an isotropic contact interaction as well as some finite-ranged and even higher partial-wave interactions [14,36–39]. Itinerant ferromagnetism induced by long-range and anisotropic dipole-dipole interaction (DDI) has been less investigated; in contrast, many unconventional quantum phases such as supersolidity [40] and charge and spin density waves [41,42] have been predicted in polar molecules $^{40}\text{K}^{87}\text{Rb}$ [43–46] and $^{23}\text{Na}^{40}\text{K}$ [47] and magnetic dipolar ^{161}Dy [48]. Apart from giving rise to the exhibition of exotic quantum phases, dipolar interaction also changed the shape of a spherical Fermi surface into a distorted one [49–53] and caused a structural second-order ferromagnetism transition [51,52]. In addition to the internal interaction, a common way of manipulating ultracold atoms is by employing the external field to induce other interacting mechanics such as spin-orbit coupling (SOC). As far as we know, SOC in condensed-matter physics whose origination is the movement of an electron in an intrinsic electric field in a crystal is crucially responsible for numerous issues including topological insulators and Majorana fermions. In cold-atom physics, SOC arises from a synthetic gauge field created by the interaction between atoms and the Raman laser field which can generate a kind of so-called Raman-induced SOC [54,55]. Recently, one- and two-dimensional SOC have been successfully achieved in Bose and Fermi gases [56–60] as well as in the dipolar fermion system [61]. Although experimental breakthroughs in quantum gas with SOC have been made in recent years, this topic of the itinerant magnetism in such systems has been rarely unraveled except for in a few works including the demonstration of an interesting chiral ferromagnetism with two-dimensional Rashba SOC and contact interaction [62–66]. In the previous work in a dipolar gas, an entrenchment of the itinerant ferromagnetism is revealed with the consideration of a one-dimensional (1D) SOC which simply entwines the z -direction momentum and spin [52]. Actually, this 1D SOC is only part of the Raman-induced SOC which contains a more cumbersome term of Raman coupling. What will contribute to the phase diagrams if a complete Raman SOC is considered is undoubtedly important to be clarified and that is what has been mainly covered in this present work.

II. MODEL

In this work, a Raman-induced SOC is considered which is simply depicted in Fig. 1(a). As shown in Fig. 1(a), a magnetic field in the z direction creates a hyperfine splitting for the spin-orbit coupling and a couple of x -direction Raman lasers that are polarized in the y and z directions interact with cold atoms, leading to an effective spin-orbit-coupled Hamiltonian [55]:

$$H_{\text{SOC}} = \frac{\hbar^2 k_x k_0}{m} \sigma_z + \frac{\delta}{2} \sigma_z + \frac{\Omega}{2} \sigma_x, \quad (1)$$

where k_0 is the wave vector of the laser, δ is the Raman detuning parameter, Ω is the Raman coupling, k_x is the x -direction momentum of the atom, and σ_x and σ_z are Pauli matrices. This effective Hamiltonian has a single-particle dispersion relation depicted in Fig. 1(b). As Raman coupling increases, the lowest double-well band evolves into a single-well shape, which, as pointed out by Ref. [67], can explain the phase

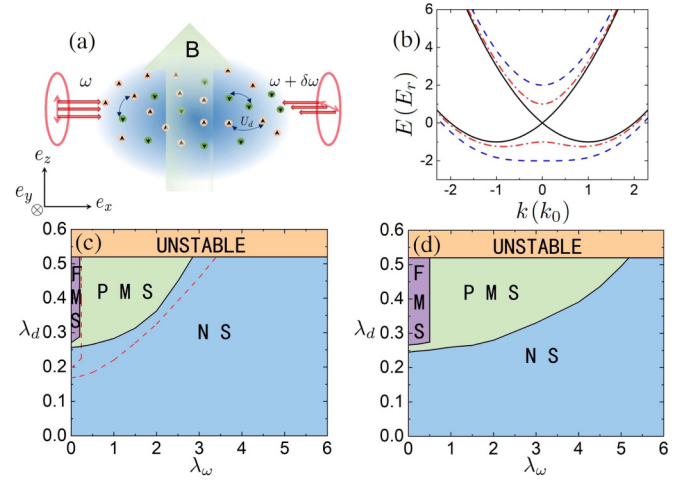


FIG. 1. (a) Schematic representation of dipolar Fermi gas with a Raman-induced spin-orbit coupling. The magnetic field B is in the z direction and a pair of Raman lasers linearly polarized in the y and z directions propagate through such an ensemble. (b) Dispersion spectrum for a Raman-induced spin-orbit-coupled system without detuning. The black solid, red dash-dotted, and blue dashed lines correspond to $\Omega = 0$, $\Omega = 2E_r$, and $\Omega = 4E_r$, where $E_r = \hbar^2 k_0^2 / (2m)$ is the recoil energy and k_0 is the wave vector of Raman lasers. (c) Zero-temperature phase diagram as a function of Raman coupling strength λ_ω and dipolar interaction λ_d , with SOC parameter $\lambda_{\text{soc}} = 1$ and contact interaction $\lambda_s = 0$. The phase diagram consists of four regions including the normal state (NS), the partially magnetic state (PMS), the fully magnetic state (FMS), and an unstable region. The dashed lines correspond to the phase boundaries shifted by a finite contact interaction $\lambda_s = 0.5$. Panel (d) is the same as panel (c), but for $\lambda_{\text{soc}} = 1.5$.

transitions among the stripe phase, the plane-wave phase, and the nonmagnetic phase in Bose gas.

The Hamiltonian for the dipolar Fermi gas consists of three parts, including the kinetic part $H_{\mathbf{k}}$, the SOC Hamiltonian H_{SOC} mentioned above, and the two-body interaction Hamiltonian H_I which includes both dipolar interaction and the contact interaction:

$$H_I = \frac{1}{2} \int d^3 \mathbf{x} d^3 \mathbf{x}' \psi_\alpha^\dagger(\mathbf{x}) \psi_\beta^\dagger(\mathbf{x}') U(\mathbf{x}, \mathbf{x}')_{\alpha\alpha', \beta\beta'} \psi_{\beta'}(\mathbf{x}') \psi_{\alpha'}(\mathbf{x}), \quad (2)$$

where ψ_α and ψ_α^\dagger are fermion annihilation and creation operator for the α component ($\alpha = 1$ and 2 represent spin-up and spin-down) and

$$U(\mathbf{x}, \mathbf{x}')_{\alpha\alpha', \beta\beta'} = \frac{d^2}{r^3} \sigma_{\alpha\alpha'}^i (\delta_{ij} - 3\hat{\mathbf{r}}_i \hat{\mathbf{r}}_j) \sigma_{\beta\beta'}^j + g \delta_{\alpha\alpha'} \delta_{\beta\beta'} \delta(\mathbf{r}), \quad (3)$$

where $\hat{\mathbf{r}} \equiv (\mathbf{x} - \mathbf{x}') / |\mathbf{x} - \mathbf{x}'|$, and d and g are the dipole moment of the fermions and the coupling strength of the contact interaction, respectively.

We have to apply a unitary transformation under which we have obtained the effective H_{SOC} to the interaction Hamiltonian H_I ,

$$H_I' = V^\dagger H_I V, \quad (4)$$

where

$$V = \begin{pmatrix} e^{-ik_0x} & 0 \\ 0 & e^{ik_0x} \end{pmatrix}. \quad (5)$$

In the following, we do the approach as

$$\begin{pmatrix} \psi'_\uparrow \\ \psi'_\downarrow \end{pmatrix} = \begin{pmatrix} e^{-ik_0x} & 0 \\ 0 & e^{ik_0x} \end{pmatrix} \begin{pmatrix} \psi_\uparrow \\ \psi_\downarrow \end{pmatrix}, \quad (6)$$

and the interaction Hamiltonian becomes

$$\begin{aligned} H_I = & \int d^3\mathbf{x}d^3\mathbf{x}' \{ \psi_\uparrow^\dagger(\mathbf{x})\psi_\uparrow^\dagger(\mathbf{x}')U(\mathbf{x},\mathbf{x}')_{\uparrow\uparrow,\uparrow\uparrow} \psi_\uparrow(\mathbf{x}')\psi_\uparrow(\mathbf{x}) + \psi_\downarrow^\dagger(\mathbf{x})\psi_\downarrow^\dagger(\mathbf{x}')U(\mathbf{x},\mathbf{x}')_{\downarrow\downarrow,\downarrow\downarrow} \psi_\downarrow(\mathbf{x}')\psi_\downarrow(\mathbf{x}) \\ & + \psi_\uparrow^\dagger(\mathbf{x})\psi_\downarrow^\dagger(\mathbf{x}')U(\mathbf{x},\mathbf{x}')_{\uparrow\uparrow,\downarrow\downarrow} \psi_\downarrow(\mathbf{x}')\psi_\uparrow(\mathbf{x}) + \psi_\downarrow^\dagger(\mathbf{x})\psi_\uparrow^\dagger(\mathbf{x}')U(\mathbf{x},\mathbf{x}')_{\downarrow\downarrow,\uparrow\uparrow} \psi_\uparrow(\mathbf{x}')\psi_\downarrow(\mathbf{x}) \\ & + [\psi_\uparrow^\dagger(\mathbf{x})\psi_\uparrow^\dagger(\mathbf{x}')U(\mathbf{x},\mathbf{x}')_{\uparrow\downarrow,\uparrow\uparrow} \psi_\uparrow(\mathbf{x}')\psi_\downarrow(\mathbf{x}) + \psi_\uparrow^\dagger(\mathbf{x})\psi_\downarrow^\dagger(\mathbf{x}')U(\mathbf{x},\mathbf{x}')_{\uparrow\downarrow,\downarrow\downarrow} \psi_\downarrow(\mathbf{x}')\psi_\downarrow(\mathbf{x})]e^{2ik_0x} \\ & + [\psi_\downarrow^\dagger(\mathbf{x})\psi_\uparrow^\dagger(\mathbf{x}')U(\mathbf{x},\mathbf{x}')_{\downarrow\uparrow,\uparrow\uparrow} \psi_\uparrow(\mathbf{x}')\psi_\uparrow(\mathbf{x}) + \psi_\downarrow^\dagger(\mathbf{x})\psi_\downarrow^\dagger(\mathbf{x}')U(\mathbf{x},\mathbf{x}')_{\downarrow\uparrow,\downarrow\downarrow} \psi_\downarrow(\mathbf{x}')\psi_\uparrow(\mathbf{x})]e^{-2ik_0x} \\ & + [\psi_\uparrow^\dagger(\mathbf{x})\psi_\uparrow^\dagger(\mathbf{x}')U(\mathbf{x},\mathbf{x}')_{\uparrow\uparrow,\uparrow\downarrow} \psi_\downarrow(\mathbf{x}')\psi_\uparrow(\mathbf{x}) + \psi_\downarrow^\dagger(\mathbf{x})\psi_\uparrow^\dagger(\mathbf{x}')U(\mathbf{x},\mathbf{x}')_{\downarrow\downarrow,\uparrow\downarrow} \psi_\downarrow(\mathbf{x}')\psi_\downarrow(\mathbf{x})]e^{2ik_0x'} \\ & + [\psi_\uparrow^\dagger(\mathbf{x})\psi_\downarrow^\dagger(\mathbf{x}')U(\mathbf{x},\mathbf{x}')_{\uparrow\uparrow,\downarrow\downarrow} \psi_\uparrow(\mathbf{x}')\psi_\uparrow(\mathbf{x}) + \psi_\downarrow^\dagger(\mathbf{x})\psi_\downarrow^\dagger(\mathbf{x}')U(\mathbf{x},\mathbf{x}')_{\downarrow\downarrow,\uparrow\downarrow} \psi_\uparrow(\mathbf{x}')\psi_\downarrow(\mathbf{x})]e^{-2ik_0x'} \\ & + \psi_\uparrow^\dagger(\mathbf{x})\psi_\uparrow^\dagger(\mathbf{x}')U(\mathbf{x},\mathbf{x}')_{\uparrow\downarrow,\uparrow\downarrow} \psi_\downarrow(\mathbf{x}')\psi_\downarrow(\mathbf{x})e^{2ik_0(x+x')} + \psi_\uparrow^\dagger(\mathbf{x})\psi_\downarrow^\dagger(\mathbf{x}')U(\mathbf{x},\mathbf{x}')_{\uparrow\downarrow,\downarrow\downarrow} \psi_\uparrow(\mathbf{x}')\psi_\downarrow(\mathbf{x})e^{2ik_0(x-x')} \\ & + \psi_\downarrow^\dagger(\mathbf{x})\psi_\uparrow^\dagger(\mathbf{x}')U(\mathbf{x},\mathbf{x}')_{\downarrow\uparrow,\uparrow\downarrow} \psi_\downarrow(\mathbf{x}')\psi_\uparrow(\mathbf{x})e^{-2ik_0(x-x')} + \psi_\downarrow^\dagger(\mathbf{x})\psi_\downarrow^\dagger(\mathbf{x}')U(\mathbf{x},\mathbf{x}')_{\downarrow\uparrow,\downarrow\downarrow} \psi_\uparrow(\mathbf{x}')\psi_\uparrow(\mathbf{x})e^{-2ik_0(x+x')} \}. \quad (7) \end{aligned}$$

Next we transform the interaction Hamiltonian of the coordinate representation above into momentum representation and we obtain

$$\begin{aligned} H_I = & \sum_{\mathbf{k}_1, \mathbf{k}_2, \mathbf{q}} [U(\mathbf{q})_{\uparrow\uparrow,\uparrow\uparrow} a_{\mathbf{k}_1,\uparrow}^\dagger a_{\mathbf{k}_2,\uparrow}^\dagger a_{\mathbf{k}_2-\mathbf{q},\uparrow} a_{\mathbf{k}_1+\mathbf{q},\uparrow} + U(\mathbf{q})_{\uparrow\uparrow,\downarrow\downarrow} a_{\mathbf{k}_1,\uparrow}^\dagger a_{\mathbf{k}_2,\downarrow}^\dagger a_{\mathbf{k}_2-\mathbf{q},\downarrow} a_{\mathbf{k}_1+\mathbf{q},\uparrow} \\ & + U(\mathbf{q})_{\downarrow\downarrow,\uparrow\uparrow} a_{\mathbf{k}_1,\downarrow}^\dagger a_{\mathbf{k}_2,\uparrow}^\dagger a_{\mathbf{k}_2-\mathbf{q},\uparrow} a_{\mathbf{k}_1+\mathbf{q},\downarrow} + U(\mathbf{q})_{\downarrow\downarrow,\downarrow\downarrow} a_{\mathbf{k}_1,\downarrow}^\dagger a_{\mathbf{k}_2,\downarrow}^\dagger a_{\mathbf{k}_2-\mathbf{q},\downarrow} a_{\mathbf{k}_1+\mathbf{q},\downarrow} \\ & + U(\mathbf{q})_{\uparrow\downarrow,\uparrow\uparrow} a_{\mathbf{k}_1,\uparrow}^\dagger a_{\mathbf{k}_2,\uparrow}^\dagger a_{\mathbf{k}_2-\mathbf{q},\uparrow} a_{\mathbf{k}_1+\mathbf{q}-2\mathbf{k}_0,\downarrow} + U(\mathbf{q})_{\uparrow\downarrow,\downarrow\downarrow} a_{\mathbf{k}_1,\uparrow}^\dagger a_{\mathbf{k}_2,\downarrow}^\dagger a_{\mathbf{k}_2-\mathbf{q},\downarrow} a_{\mathbf{k}_1+\mathbf{q}-2\mathbf{k}_0,\downarrow} \\ & + U(\mathbf{q})_{\downarrow\uparrow,\uparrow\uparrow} a_{\mathbf{k}_1,\downarrow}^\dagger a_{\mathbf{k}_2,\uparrow}^\dagger a_{\mathbf{k}_2-\mathbf{q},\uparrow} a_{\mathbf{k}_1+\mathbf{q}+2\mathbf{k}_0,\uparrow} + U(\mathbf{q})_{\downarrow\uparrow,\downarrow\downarrow} a_{\mathbf{k}_1,\downarrow}^\dagger a_{\mathbf{k}_2,\downarrow}^\dagger a_{\mathbf{k}_2-\mathbf{q},\downarrow} a_{\mathbf{k}_1+\mathbf{q}+2\mathbf{k}_0,\uparrow} \\ & + U(\mathbf{q})_{\uparrow\uparrow,\uparrow\downarrow} a_{\mathbf{k}_1,\uparrow}^\dagger a_{\mathbf{k}_2,\uparrow}^\dagger a_{\mathbf{k}_2-\mathbf{q}-2\mathbf{k}_0,\downarrow} a_{\mathbf{k}_1+\mathbf{q},\uparrow} + U(\mathbf{q})_{\downarrow\downarrow,\uparrow\downarrow} a_{\mathbf{k}_1,\downarrow}^\dagger a_{\mathbf{k}_2,\uparrow}^\dagger a_{\mathbf{k}_2-\mathbf{q}-2\mathbf{k}_0,\downarrow} a_{\mathbf{k}_1+\mathbf{q},\downarrow} \\ & + U(\mathbf{q})_{\uparrow\uparrow,\downarrow\downarrow} a_{\mathbf{k}_1,\uparrow}^\dagger a_{\mathbf{k}_2,\downarrow}^\dagger a_{\mathbf{k}_2-\mathbf{q}+2\mathbf{k}_0,\uparrow} a_{\mathbf{k}_1+\mathbf{q},\uparrow} + U(\mathbf{q})_{\downarrow\downarrow,\uparrow\downarrow} a_{\mathbf{k}_1,\downarrow}^\dagger a_{\mathbf{k}_2,\downarrow}^\dagger a_{\mathbf{k}_2-\mathbf{q}+2\mathbf{k}_0,\uparrow} a_{\mathbf{k}_1+\mathbf{q},\downarrow} \\ & + U(\mathbf{q})_{\uparrow\downarrow,\uparrow\downarrow} a_{\mathbf{k}_1,\uparrow}^\dagger a_{\mathbf{k}_2,\uparrow}^\dagger a_{\mathbf{k}_2-\mathbf{q}-2\mathbf{k}_0,\downarrow} a_{\mathbf{k}_1+\mathbf{q}-2\mathbf{k}_0,\downarrow} + U(\mathbf{q})_{\uparrow\downarrow,\downarrow\downarrow} a_{\mathbf{k}_1,\uparrow}^\dagger a_{\mathbf{k}_2,\downarrow}^\dagger a_{\mathbf{k}_2-\mathbf{q}+2\mathbf{k}_0,\uparrow} a_{\mathbf{k}_1+\mathbf{q}-2\mathbf{k}_0,\downarrow} \\ & + U(\mathbf{q})_{\downarrow\uparrow,\uparrow\downarrow} a_{\mathbf{k}_1,\downarrow}^\dagger a_{\mathbf{k}_2,\uparrow}^\dagger a_{\mathbf{k}_2-\mathbf{q}-2\mathbf{k}_0,\downarrow} a_{\mathbf{k}_1+\mathbf{q}+2\mathbf{k}_0,\uparrow} + U(\mathbf{q})_{\downarrow\uparrow,\downarrow\downarrow} a_{\mathbf{k}_1,\downarrow}^\dagger a_{\mathbf{k}_2,\downarrow}^\dagger a_{\mathbf{k}_2-\mathbf{q}+2\mathbf{k}_0,\uparrow} a_{\mathbf{k}_1+\mathbf{q}+2\mathbf{k}_0,\uparrow}], \quad (8) \end{aligned}$$

where $\mathbf{k}_0 = (k_0, 0, 0)$ and

$$U(\mathbf{q})_{\alpha\alpha',\beta\beta'} = \frac{4\pi d^2}{3} \sigma_{\alpha\alpha'}^i (3\hat{\mathbf{q}}_i \hat{\mathbf{q}}_j - \delta_{i,j}) \sigma_{\beta\beta'}^j + g \delta_{\alpha,\alpha'} \delta_{\beta,\beta'}. \quad (9)$$

The results above include a few momentum-nonconservation terms which we can ignore in the following calculation for the reason that we are dealing with a homogeneous gas. After a mean-field approximation and bringing in a few symbols $n_{\mathbf{k},\alpha} = \langle a_{\mathbf{k},\alpha}^\dagger a_{\mathbf{k},\alpha} \rangle$ representing the particle density of spin-up and spin-down in momentum space and $t_{\mathbf{k}} = \langle a_{\mathbf{k},\uparrow}^\dagger a_{\mathbf{k},\downarrow} \rangle$ representing the spin-flip density, the total Hamiltonian has the simple form of

$$H = \sum_{\mathbf{k}} \begin{pmatrix} a_{\mathbf{k},\uparrow}^\dagger & a_{\mathbf{k},\downarrow}^\dagger \end{pmatrix} \begin{pmatrix} \epsilon_1(\mathbf{k}) & \epsilon_3(\mathbf{k}) \\ \epsilon_3(\mathbf{k}) & \epsilon_2(\mathbf{k}) \end{pmatrix} \begin{pmatrix} a_{\mathbf{k},\uparrow} \\ a_{\mathbf{k},\downarrow} \end{pmatrix}, \quad (10)$$

where

$$\begin{aligned} \epsilon_1(\mathbf{k}) = & \frac{\hbar^2 \mathbf{k}^2}{2m} + \frac{\hbar^2 k_0}{m} k_x + \frac{g}{V} \sum_{\mathbf{k}'} n_{\mathbf{k}',\downarrow} + \sum_{\mathbf{k}'} \frac{2\pi d^2}{3V} \\ & \times [(3 \cos^2 \theta_{\mathbf{k}-\mathbf{k}'+2\mathbf{k}_0} - 1) n_{\mathbf{k}',\downarrow} + (3 \cos^2 \theta_{\mathbf{k}-\mathbf{k}'-2\mathbf{k}_0} - 1) \\ & \times n_{\mathbf{k}',\downarrow} - 2 * (3 \cos^2 \theta_{\mathbf{k}-\mathbf{k}'} - 1) n_{\mathbf{k}',\uparrow}], \quad (11) \end{aligned}$$

$$\begin{aligned} \epsilon_2(\mathbf{k}) = & \frac{\hbar^2 \mathbf{k}^2}{2m} - \frac{\hbar^2 k_0}{m} k_x + \frac{g}{V} \sum_{\mathbf{k}'} n_{\mathbf{k}',\uparrow} \\ & + \sum_{\mathbf{k}'} \frac{2\pi d^2}{3V} [(3 \cos^2 \theta_{\mathbf{k}-\mathbf{k}'+2\mathbf{k}_0} - 1) n_{\mathbf{k}',\uparrow} \\ & + (3 \cos^2 \theta_{\mathbf{k}-\mathbf{k}'-2\mathbf{k}_0} - 1) n_{\mathbf{k}',\uparrow} - 2 * \\ & \times (3 \cos^2 \theta_{\mathbf{k}-\mathbf{k}'} - 1) n_{\mathbf{k}',\downarrow}], \quad (12) \end{aligned}$$

$$\epsilon_3(\mathbf{k}) = \frac{\Omega}{2} - \frac{g}{V} \sum_{\mathbf{k}'} t_{\mathbf{k}'} + \sum_{\mathbf{k}'} \frac{4\pi d^2}{3V} (3 \cos^2 \theta_{\mathbf{k}-\mathbf{k}'} - 1) t_{\mathbf{k}'}. \quad (13)$$

After a canonical transformation we obtain the total Hamiltonian of the following form:

$$H = \sum_{\mathbf{k}} (b_{\mathbf{k},\uparrow}^\dagger, b_{\mathbf{k},\downarrow}^\dagger) \begin{pmatrix} \xi_1(\mathbf{k}) & 0 \\ 0 & \xi_2(\mathbf{k}) \end{pmatrix} \begin{pmatrix} b_{\mathbf{k},\uparrow} \\ b_{\mathbf{k},\downarrow} \end{pmatrix}, \quad (14)$$

where $b_{\mathbf{k}}^\dagger$ and $b_{\mathbf{k}}$ are creation and annihilation operators of the quasiparticles and

$$\xi_1(\mathbf{k}) = u(\mathbf{k})^2 \epsilon_1(\mathbf{k}) + v(\mathbf{k})^2 \epsilon_2(\mathbf{k}) + 2u(\mathbf{k})v(\mathbf{k})\epsilon_3(\mathbf{k}), \quad (15)$$

$$\xi_2(\mathbf{k}) = v(\mathbf{k})^2 \epsilon_1(\mathbf{k}) + u(\mathbf{k})^2 \epsilon_2(\mathbf{k}) + 2u(\mathbf{k})v(\mathbf{k})\epsilon_3(\mathbf{k}), \quad (16)$$

$$u(\mathbf{k})^2, v(\mathbf{k})^2 = 1/2 \pm \frac{\epsilon_1(\mathbf{k}) - \epsilon_2(\mathbf{k})}{2\sqrt{[\epsilon_1(\mathbf{k}) - \epsilon_2(\mathbf{k})]^2 + 4\epsilon_3(\mathbf{k})^2}}. \quad (17)$$

The density distribution $n_{\mathbf{k},\alpha}$, spin-flip $t_{\mathbf{k}}$, and chemical potential μ can be calculated self-consistently with the help of the following equations:

$$n_{\mathbf{k},\uparrow} = u(\mathbf{k})^2 f(\xi_1(\mathbf{k})) + v(\mathbf{k})^2 f(\xi_2(\mathbf{k})), \quad (18)$$

$$n_{\mathbf{k},\downarrow} = v(\mathbf{k})^2 f(\xi_1(\mathbf{k})) + u(\mathbf{k})^2 f(\xi_2(\mathbf{k})), \quad (19)$$

$$N = \sum_{\mathbf{k}} (n_{\mathbf{k},\uparrow} + n_{\mathbf{k},\downarrow}), \quad (20)$$

$$t_{\mathbf{k}} = u(\mathbf{k})v(\mathbf{k})[f(\xi_1(\mathbf{k})) - f(\xi_2(\mathbf{k}))], \quad (21)$$

$$f(x) = \frac{1}{e^{(x-\mu)/k_B T} + 1}. \quad (22)$$

We introduce the dimensionless parameters including the dipolar interaction parameter $\lambda_d = nd^2/\epsilon_F$, the SOC parameter $\lambda_{\text{soc}} = k_0/k_F$, the contact interaction parameter $\lambda_s = gn/\epsilon_F$, the Raman coupling parameter $\lambda_\omega = \Omega/\epsilon_F$, and the temperature parameter $\lambda_T = k_B T/\epsilon_F$, where ϵ_F , k_F , and k_B are the Fermi energy, the Fermi wave vector, and the Boltzmann constant, respectively. Then the consistent equations can become dimensionless and be calculated numerically.

III. RESULTS

Our calculation indicates that ferromagnetism phase transition can occur under suitable parameters. We plot the phase diagrams as functions of λ_d , λ_ω , and λ_{soc} shown in Figs. 1 and 2. An apparent conclusion can be drawn that the Raman spin-flip effect can eliminate the tendency to ferromagnetic transition. The competition between dipolar interaction and Raman coupling might seem strange because spin-flip could intuitively imbalance the atoms of spin-up and spin-down, thus favoring a ferromagnetic state. However, as we think further, the ground state should be a Hartree-Fock state with the following form:

$$\psi(\mathbf{r}_1, \dots, \mathbf{r}_N) = \sum_P \frac{(-1)^P}{\sqrt{N!}} \phi_1(\mathbf{r}_1) \phi_2(\mathbf{r}_2) \dots \phi_N(\mathbf{r}_N), \quad (23)$$

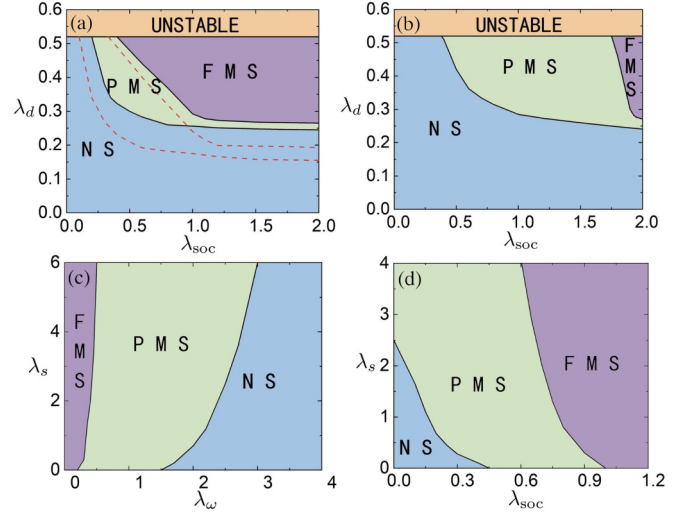


FIG. 2. (a) Zero-temperature phase diagram as functions of SOC strength λ_{soc} and dipolar interaction λ_d with $\lambda_\omega = 0.2$ and $\lambda_s = 0$. The dashed lines correspond to the phase boundaries shifted by a finite contact interaction $\lambda_s = 0.5$. Panel (b) is the same as panel (a), but for $\lambda_\omega = 1$. (c) Phase diagrams as functions of contact interaction λ_s and Raman coupling strength λ_ω with $\lambda_{\text{soc}} = 1$. (d) Phase diagrams as functions of contact interaction λ_s and SOC strength λ_{soc} with $\lambda_\omega = 0.2$. Both panels (c) and (d) are for $\lambda_d = 0.3$.

where P is an arbitrary permutation. For instance, if we take $N = 2$, the total wave function with spin freedom will become $\psi(\mathbf{r}_1, \mathbf{r}_2, \alpha, \beta) = \frac{1}{\sqrt{2}}[\phi_1(\mathbf{r}_1, \alpha)\phi_2(\mathbf{r}_2, \beta) - \phi_2(\mathbf{r}_1, \beta)\phi_1(\mathbf{r}_2, \alpha)]$. For a symmetry-broken ferromagnetic state, the wave function can be certainly written down as $\psi(\mathbf{r}_1, \mathbf{r}_2, \uparrow, \uparrow)$. If we regard the spin-flip term as an operator \hat{F} satisfying $\hat{F}|\uparrow\rangle = |\downarrow\rangle$, $\hat{F}|\downarrow\rangle = |\uparrow\rangle$, then \hat{F} has a zero expectation with $\psi(\mathbf{r}_1, \mathbf{r}_2, \uparrow, \uparrow)$. For a normal state ($S = 0$), the wave function of the spin part must be an antisymmetric spin singlet, and the whole wave function turns out to be a combination of $\psi(\mathbf{r}_1, \mathbf{r}_2, \uparrow, \downarrow)$ and $\psi(\mathbf{r}_1, \mathbf{r}_2, \downarrow, \uparrow)$, which will add a minus if we exchange spin-up and spin-down and the expectation of \hat{F} is also not zero with this state. The analysis above can be certainly generalized to a many-particle system. For a many-particle system, the expectation is that \hat{F} is zero even in a partially ferromagnetic state and has a nonzero value only in a symmetric normal state. Thus a system with a spin-flip term favors a nonferromagnetic phase. This effect can be also an analogy with the magnetic-nonmagnetic quantum phase transition as Raman coupling increases in a bosonic spin-orbit-coupled system [67].

It is also interesting from the phase diagrams of Fig. 2 that the 1D SOC can enhance the ferromagnetism with a saturation, which can be seen from a rough calculation of the dipolar energy which takes the form of $(\mathbf{d}_1 \cdot \mathbf{d}_2)/r^3 - (\mathbf{d}_1 \cdot \mathbf{r})(\mathbf{d}_2 \cdot \mathbf{r})/r^5$, where \mathbf{d}_1 , \mathbf{d}_2 , and \mathbf{r} are dipole moments and the separation of two dipoles. If we equally cast the dipoles of spin-up and spin-down into a spherical region, the interspecies DDI and the intraspecies DDI cancel out. But if we separate two identical spherical balls each filled with dipoles of different spins, the interspecies DDI approaches zero as the distance between two balls becomes large enough with the remaining intraspecies DDI being a constant value. At a sufficiently large

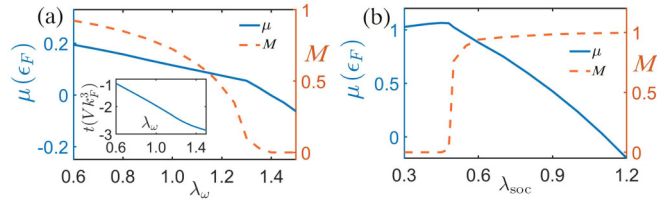


FIG. 3. (a) Zero-temperature chemical potential μ (blue solid line) and magnetization M (orange dashed line) as functions of Raman coupling strength λ_ω with $\lambda_{\text{soc}} = 1$. The inset shows the total spin-flip $t = \sum_{\mathbf{k}} \langle a_{\mathbf{k},\uparrow}^\dagger a_{\mathbf{k},\downarrow} \rangle$ as a function of λ_ω . (b) Zero-temperature chemical potential μ (blue solid line) and magnetization M (orange dashed line) as functions of λ_{soc} with $\lambda_\omega = 0.2$. Both panels (a) and (b) are obtained with $\lambda_d = 0.30$ and $\lambda_s = 0.1$.

1D SOC, Fermi surfaces are well separated in momentum space, under which the difference of total DDI between a normal state and a ferromagnetic state will saturate with the separation of Fermi surfaces.

The detail of the ferromagnetic transition is analyzed by plotting the chemical potential and magnetization as displayed in Fig. 3. The derivations of chemical potential at transition points behave discontinuously, manifesting a first-order ferromagnetic phase transition. The order parameters $n_{\mathbf{k},\uparrow}$ and $n_{\mathbf{k},\downarrow}$ are depicted in Fig. 4 and have a rotational symmetry. Quite contrary to an ideal spherically Fermi surface, the distribution of particles in momentum space shows a distorted shape because of the presence of anisotropic dipolar interaction. On the other hand, the shapes of Fermi surfaces are also influenced by the Raman coupling strength whose detail can be referred to Fig. 5. Generally speaking, spin-flip can gradually connect the disjointed Fermi surfaces as displayed in Fig. 5, while dipolar interaction can distort Fermi surfaces. Interestingly, Raman coupling leads to a nonzero spin-flip $t_{\mathbf{k}}$ which has

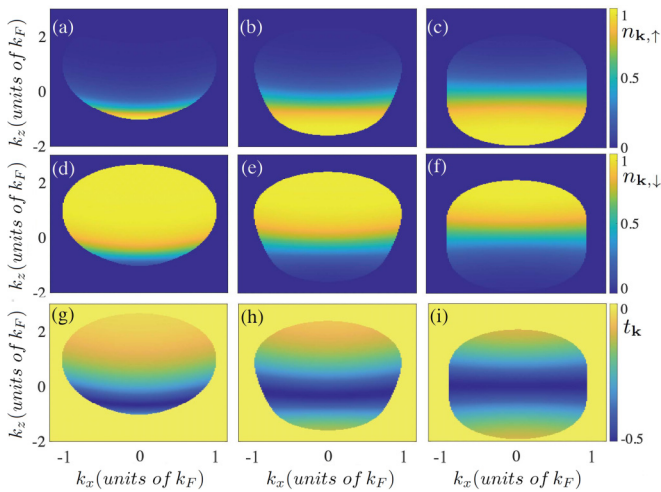


FIG. 4. Zero-temperature density distributions $n_{\mathbf{k},\uparrow}$ [panels (a)–(c)] and $n_{\mathbf{k},\downarrow}$ [panels (d)–(f)] and spin-flip distribution $t_{\mathbf{k}}$ [panels (g)–(i)] with $\lambda_{\text{soc}} = 1$, $\lambda_s = 0.1$, and $\lambda_d = 0.30$. Panels (a), (d), and (g) are for $\lambda_\omega = 0.8$; panels (b), (e), and (h) are for $\lambda_\omega = 1.2$; and panels (c), (f), and (i) are for $\lambda_\omega = 1.45$. These figures from the left column to the right column show a transition from a ferromagnetic state to a normal state.

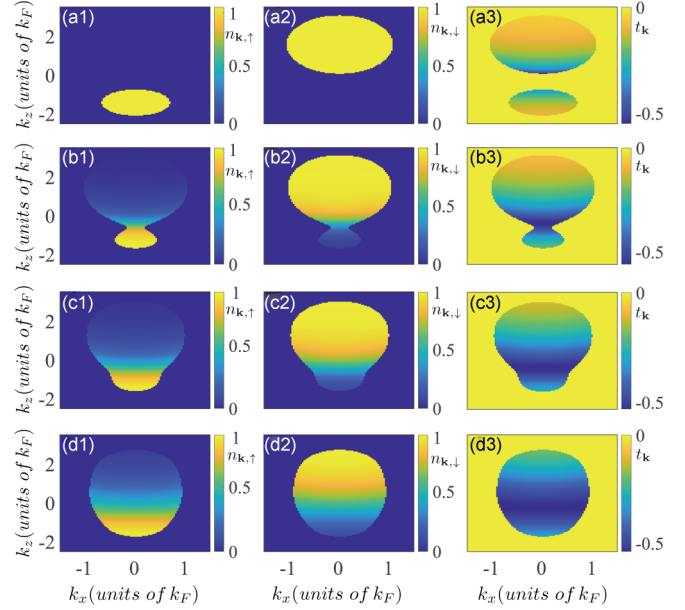


FIG. 5. Density distribution of the spin-up component $n_{\mathbf{k},\uparrow}$ [panels (a1)–(d1)], the spin-down component $n_{\mathbf{k},\downarrow}$ [panels (a2)–(d2)], and the spin-flip distribution $t_{\mathbf{k}} = \langle a_{\mathbf{k},\uparrow}^\dagger a_{\mathbf{k},\downarrow} \rangle$ [panels (a3)–(d3)] with $\lambda_{\text{soc}} = 1$ and $\lambda_s = 0$. Panels (a1)–(a3) are for $\lambda_\omega = 0.2$ and $\lambda_d = 0.255$; panels (b1)–(b3) are for $\lambda_\omega = 2.0$ and $\lambda_d = 0.3$; panels (c1)–(c3) for $\lambda_\omega = 3.0$ and $\lambda_d = 0.355$; and panels (d1)–(d3) are for $\lambda_\omega = 4.5$ and $\lambda_d = 0.45$.

a nonuniform distribution in momentum space as shown in Fig. 6. The total spin-flip $t = \sum_{\mathbf{k}} t_{\mathbf{k}}$ is a negative value and declines monotonously as λ_ω increases, which is displayed in Fig. 3. We can regard this spin-flip distribution as a symmetry “gate” through which particles of spin-up can accumulate and particles of spin-down can escape. As λ_ω increases further,

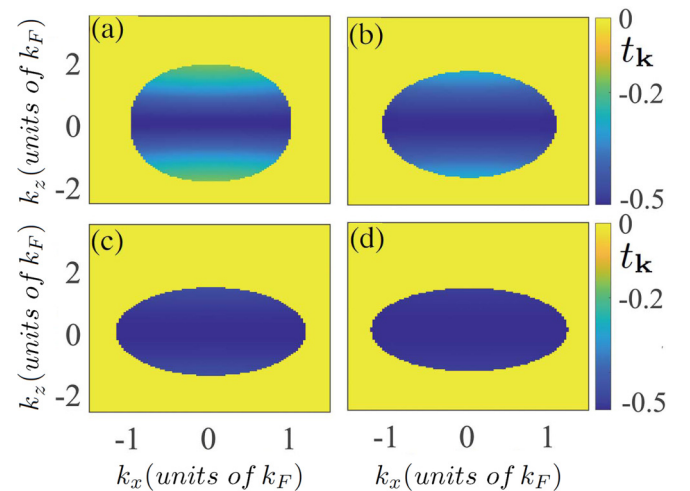


FIG. 6. Spin-flip distribution $t_{\mathbf{k}} = \langle a_{\mathbf{k},\uparrow}^\dagger a_{\mathbf{k},\downarrow} \rangle$ when Raman coupling gradually increases with $\lambda_{\text{soc}} = 1$, $\lambda_s = 0.1$, and $\lambda_d = 0.3$. Panel (a) is for $\lambda_\omega = 2$, panel (b) is for $\lambda_\omega = 3$, panel (c) is for $\lambda_\omega = 6$, and panel (d) is for $\lambda_\omega = 9$. With an increasing λ_ω , the spin-flip distribution in momentum space becomes more uniform and attains up to a saturation of -0.5 .

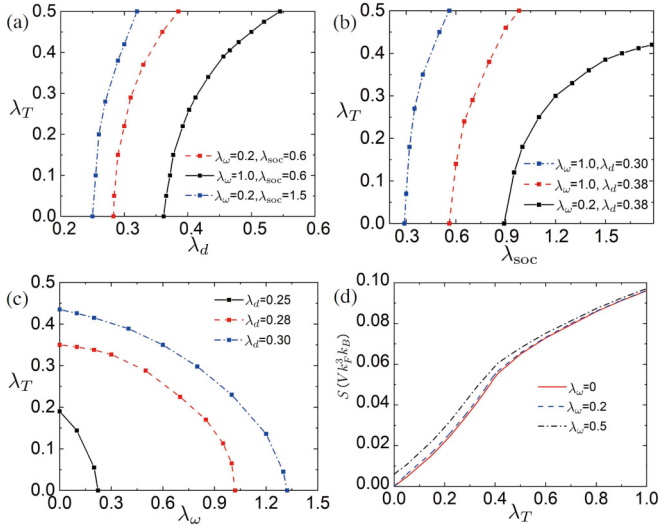


FIG. 7. Ferromagnetic transition temperature as functions of dipolar interaction λ_d (a), SOC parameter λ_{soc} (b), and Raman coupling strength λ_ω (c). Panels (a) and (b) are for $\lambda_s = 0$ and panel (c) is for $\lambda_s = 0.1$ and $\lambda_{\text{soc}} = 1$. (d) Entropy as a function of temperature λ_T with $\lambda_d = 0.30$, $\lambda_{\text{soc}} = 1$, and $\lambda_s = 0.1$.

this “gate” becomes more widespread, which makes the zero-temperature ground state a pseudosymmetric one different from the general Pauli paramagnetic state. Here we have to specify the pseudosymmetric normal state in our phase diagrams as a combination of a true normal state ($S = 0$) and an x -direction-polarized state. A true normal state minimizes the kinetic energy and an x -direction-polarized state minimizes the Raman coupling energy. Thus as λ_ω increases, the ground state should be a combination of an actually normal state and an x -direction-polarized state which minimizes the total energy.

As the dipolar interaction increases, a dynamical unstable property is displayed. In this unstable region, compressibility $K^{-1} = n(\partial P/\partial n)$, where pressure $P = -(\partial E/\partial V)_N$ becomes negative. When this system becomes unstable, K^{-1} changes into a negative value from a positive value and passes through zero, which manifests a divergency. What has to be pointed out is that the boundary line of the dynamical unstable region does not rely on λ_ω or λ_{soc} and is hammered at $\lambda_d \approx 0.52$ [51], which can be inferred from the following facts. When λ_ω is small enough, the state near the unstable boundary is a fully magnetic state and $t_{\mathbf{k}}$ equals zero, thus leading to no contribution to the total energy. When λ_ω is large enough, the state near the unstable boundary is a fully x -direction-polarized state and $t = \sum_{\mathbf{k}} t_{\mathbf{k}}$ is a constant. The energy of the Raman coupling part takes the form of $\Omega V k_F^3 t$, whose second derivative to n is zero, thus also making no contribution to compressibility. As for the intermediate region, the Raman coupling term equals an x -direction-exerted magnetic field and does not influence the intrinsic unstable properties as we have argued in my previous paper [52] that a momentum-dependent magnetic field in z direction does not change the unstable region. In Fig. 7, we plot the ferromagnetic transition temperatures as functions of λ_d , λ_{soc} , and λ_ω . The transition

temperature increases with λ_d and λ_{soc} and declines with λ_ω . Finally, it is also of great interest to know how entropy behaves at finite temperature, which takes the form of $S = -k_B \sum_{\mathbf{k}} \{f(\mathbf{k}) \ln f(\mathbf{k}) + [1 - f(\mathbf{k})] \ln [1 - f(\mathbf{k})]\}$.

As displayed in Fig. 7(d), entropy increases as temperature increases, which agrees with our general knowledge. What may seem strange to us is that the residual entropy at zero temperature does not always approach zero when altering the Raman coupling parameter. We speculatively attribute this to be an illusive quantum fluctuation which reflects some deficiencies in the mean-field approximation used in the work.

IV. CONCLUSION

In most of the previous experiments, two-component fermions were usually a mixture of ultracold ^6Li atoms [5,9,10] in which the system could be cooled down to about $0.1T_F$ to $1T_F$. By tuning the effective scattering length a_s through the Feshbach resonance, a strong repulsive branch could be reached in which a Stoner-type itinerant ferromagnetism could be possibly verified. In a recent Raman spin-orbit-coupled dipolar ^{161}Dy system [61], the Zeeman sublevels of $|\downarrow\rangle \equiv |F = 21/2, m_F = -21/2\rangle$ and $|\uparrow\rangle \equiv |F = 21/2, m_F = -19/2\rangle$ were coupled by two Raman lasers with wavelength $\lambda = 741$ nm. The parameters of λ_ω and λ_{soc} are about 1 and 0.4 with a peak density of 10^{14} cm^{-3} . The dipolar interaction parameter λ_d is about 0.02 and the temperature λ_T ranges from 0.1 to 0.4. By using a scattering theory, the main results of the dipolar ^{161}Dy [61] gas were well explained consistently. Besides, the early theoretical predictions of the deformation of Fermi surfaces were also verified from a momentum distribution image [61]. In our work to observe this ferromagnetic transition demonstrated, apart from manipulating the Raman lasers, we can manage to increase the effective dipolar interaction. For instance, a three-dimensional molecular quantum gas with tunable dipolar interaction [68] was successfully evaporatively cooled by performing an electric-field-induced shielding resonance technique which was based on the theory that the elastic collision and the cooling rates had a dependence on the angle between the dipole and the heating direction. This tunability of the dipolar interaction in this system provides a great platform to attest many of the previous theoretical predictions. To observe a spin polarization experimentally, monitoring the suppression of collision could be an adopted way as collisions would be forbidden in a fully ferromagnetic state [5]. Otherwise a probing of the spin-dipole dynamics can also demonstrate the spin susceptibility [9].

In summary, we have investigated the itinerant ferromagnetic phase transition in a Raman-induced spin-orbit-coupled dipolar Fermi gas, which is mainly dominated by the long-range dipole-dipole interaction. The presence of Raman-induced spin-orbit coupling makes great contributions to the formation of the itinerant ferromagnetism and provides us a feasible tool with which to manipulate the system. The long-range dipole-dipole interaction and the spin-orbit coupling also bring us interesting physical mechanisms, for instance, the deformations of Fermi surfaces and novel spin-flip distributions.

ACKNOWLEDGMENTS

This work was supported by the National Key R&D Program of China under Grants No. 2021YFA1400900,

No. 2021YFA0718300, No. 2021YFA1400243, and No. 2021YFA0718300 and by the NSFC under Grants No. 61835013 and No. 12174461.

-
- [1] E. C. Stoner, *London, Edinburgh, Dublin Philos. Mag. J. Sci.* **15**, 1018 (1933).
- [2] E. C. Stoner, *Proc. R. Soc. London, Ser. A* **165**, 372 (1938).
- [3] Y. Nagaoka, *Phys. Rev.* **147**, 392 (1966).
- [4] H. Tasaki, *Phys. Rev. Lett.* **69**, 1608 (1992).
- [5] G.-B. Jo, Y.-R. Lee, J.-H. Choi, C. A. Christensen, T. H. Kim, J. H. Thywissen, D. E. Pritchard, and W. Ketterle, *Science* **325**, 1521 (2009).
- [6] M. C. Gutzwiller, *Phys. Rev. Lett.* **10**, 159 (1963).
- [7] H. Zhai, *Phys. Rev. A* **80**, 051605(R) (2009).
- [8] X. Cui and H. Zhai, *Phys. Rev. A* **81**, 041602(R) (2010).
- [9] G. Valtolina, F. Scazza, A. Amico, A. Burchianti, A. Recati, T. Enss, M. Inguscio, M. Zaccanti, and G. Roati, *Nat. Phys.* **13**, 704 (2017).
- [10] C. Sanner, E. J. Su, W. Huang, A. Keshet, J. Gillen, and W. Ketterle, *Phys. Rev. Lett.* **108**, 240404 (2012).
- [11] R. A. Duine and A. H. MacDonald, *Phys. Rev. Lett.* **95**, 230403 (2005).
- [12] L. He and X.-G. Huang, *Phys. Rev. A* **85**, 043624 (2012).
- [13] L. He, X.-J. Liu, X.-G. Huang, and H. Hu, *Phys. Rev. A* **93**, 063629 (2016).
- [14] L. He, *Ann. Phys.* **351**, 477 (2014).
- [15] G. J. Conduit, A. G. Green, and B. D. Simons, *Phys. Rev. Lett.* **103**, 207201 (2009).
- [16] S. Pilati, G. Bertainia, S. Giorgini, and M. Troyer, *Phys. Rev. Lett.* **105**, 030405 (2010).
- [17] S.-Y. Chang, M. Randeria, and N. Trivedi, *Proc. Natl. Acad. Sci. U.S.A.* **108**, 51 (2011).
- [18] T. Comparin, R. Bombín, M. Holzmann, F. Mazzanti, J. Boronat, and S. Giorgini, *Phys. Rev. A* **99**, 043609 (2019).
- [19] I. Zintchenko, L. Wang, and M. Troyer, *Eur. Phys. J. B* **89**, 1 (2016).
- [20] G. J. Conduit and E. Altman, *Phys. Rev. A* **83**, 043618 (2011).
- [21] D. Pekker, M. Babadi, R. Sensarma, N. Zinner, L. Pollet, M. W. Zwierlein, and E. Demler, *Phys. Rev. Lett.* **106**, 050402 (2011).
- [22] I. Sodemann, D. A. Pesin, and A. H. MacDonald, *Phys. Rev. A* **85**, 033628 (2012).
- [23] X.-J. Liu and H. Hu, *Phys. Rev. A* **82**, 043626 (2010).
- [24] P. Massignan and G. M. Bruun, *Eur. Phys. J. D* **65**, 83 (2011).
- [25] P. Massignan, M. Zaccanti, and G. M. Bruun, *Rep. Prog. Phys.* **77**, 034401 (2014).
- [26] P. Massignan, Z. Yu, and G. M. Bruun, *Phys. Rev. Lett.* **110**, 230401 (2013).
- [27] X. Cui and T.-L. Ho, *Phys. Rev. Lett.* **110**, 165302 (2013).
- [28] C. W. von Keyserlingk and G. J. Conduit, *Phys. Rev. A* **83**, 053625 (2011).
- [29] P. T. Grochowski, T. Karpiuk, M. Brewczyk, and K. Rzażewski, *Phys. Rev. Lett.* **119**, 215303 (2017).
- [30] R. A. Duine, M. Polini, H. T. C. Stoof, and G. Vignale, *Phys. Rev. Lett.* **104**, 220403 (2010).
- [31] A. Recati and S. Stringari, *Phys. Rev. Lett.* **106**, 080402 (2011).
- [32] G. J. Conduit and E. Altman, *Phys. Rev. A* **82**, 043603 (2010).
- [33] J. Ryszkiewicz, M. Brewczyk, and T. Karpiuk, *Phys. Rev. A* **101**, 013618 (2020).
- [34] M. Sandri, A. Minguzzi, and F. Toigo, *Europhys. Lett.* **96**, 66004 (2011).
- [35] H. Tajima and K. Iida, *J. Phys. Soc. Jpn.* **90**, 024004 (2021).
- [36] Z. Sun and Q. Gu, *J. Phys. B: At. Mol. Phys.* **50**, 015302 (2017).
- [37] F. Arias de Saavedra, F. Mazzanti, J. Boronat, and A. Polls, *Phys. Rev. A* **85**, 033615 (2012).
- [38] C. W. von Keyserlingk and G. J. Conduit, *Phys. Rev. B* **87**, 184424 (2013).
- [39] E. Vermeyen, C. A. R. Sá de Melo, and J. Tempere, *Phys. Rev. A* **98**, 023635 (2018).
- [40] T.-S. Zeng and L. Yin, *Phys. Rev. B* **89**, 174511 (2014).
- [41] Z. Wu, J. K. Block, and G. M. Bruun, *Phys. Rev. B* **91**, 224504 (2015).
- [42] S. G. Bhongale, L. Mathey, S.-W. Tsai, C. W. Clark, and E. Zhao, *Phys. Rev. A* **87**, 043604 (2013).
- [43] K.-K. Ni, S. Ospelkaus, M. H. G. de Miranda, A. Pe'Er, B. Neyenhuis, J. J. Zirbel, S. Kotochigova, P. S. Julienne, D. S. Jin, and J. Ye, *Science* **322**, 231 (2008).
- [44] Y. Bo, S. A. Moses, G. Bryce, J. P. Covey, K. R. A. Hazzard, R. Ana Maria, D. S. Jin, and Y. Jun, *Nature (London)* **501**, 521 (2013).
- [45] A. Chotia, B. Neyenhuis, S. A. Moses, B. Yan, J. P. Covey, M. Foss-Feig, A. M. Rey, D. S. Jin, and J. Ye, *Phys. Rev. Lett.* **108**, 080405 (2012).
- [46] K.-K. Ni, S. Ospelkaus, D. Wang, G. Quémener, B. Neyenhuis, M. H. G. de Miranda, J. L. Bohn, J. Ye, and D. S. Jin, *Nature (London)* **464**, 1324 (2010).
- [47] C.-H. Wu, J. W. Park, P. Ahmadi, S. Will, and M. W. Zwierlein, *Phys. Rev. Lett.* **109**, 085301 (2012).
- [48] M. Lu, N. Q. Burdick, and B. L. Lev, *Phys. Rev. Lett.* **108**, 215301 (2012).
- [49] T. Miyakawa, T. Sogo, and H. Pu, *Phys. Rev. A* **77**, 061603(R) (2008).
- [50] S. Ronen and J. L. Bohn, *Phys. Rev. A* **81**, 033601 (2010).
- [51] B. M. Fregoso and E. Fradkin, *Phys. Rev. Lett.* **103**, 205301 (2009).
- [52] X.-J. Feng and L. Yin, *Chin. Phys. Lett.* **37**, 020301 (2020).
- [53] X.-J. Feng and L. Yin, *Chin. Phys. B* **29**, 110306 (2020).
- [54] J. Dalibard, F. Gerbier, G. Juzeliūnas, and P. Öhberg, *Rev. Mod. Phys.* **83**, 1523 (2011).
- [55] H. Zhai, *Rep. Prog. Phys.* **78**, 026001 (2015).
- [56] Y.-J. Lin, K. Jiménez-García, and I. B. Spielman, *Nature (London)* **471**, 83 (2011).
- [57] P. Wang, Z.-Q. Yu, Z. Fu, J. Miao, L. Huang, S. Chai, H. Zhai, and J. Zhang, *Phys. Rev. Lett.* **109**, 095301 (2012).
- [58] Z. Wu, L. Zhang, W. Sun, X. T. Xu, B. Z. Wang, S. C. Ji, Y. Deng, S. Chen, X. J. Liu, and J. W. Pan, *Science* **354**, 83 (2016).
- [59] Z. Meng, L. Huang, P. Peng, D. Li, L. Chen, Y. Xu, C. Zhang, P. Wang, and J. Zhang, *Phys. Rev. Lett.* **117**, 235304 (2016).

- [60] L. Huang, Z. Meng, P. Wang, P. Peng, S.-L. Zhang, L. Chen, D. Li, Q. Zhou, and J. Zhang, *Nat. Phys.* **12**, 540 (2016).
- [61] N. Q. Burdick, Y. Tang, and B. L. Lev, *Phys. Rev. X* **6**, 031022 (2016).
- [62] W. E. Liu, S. Chesi, D. Webb, U. Zülicke, R. Winkler, R. Joynt, and D. Culcer, *Phys. Rev. B* **96**, 235425 (2017).
- [63] S.-S. Zhang, W.-M. Liu, and H. Pu, *Phys. Rev. A* **93**, 043602 (2016).
- [64] H. Vivas C., *J. Magn. Magn. Mater.* **498**, 166113 (2020).
- [65] R. Liao, Y. Yi-Xiang, and W.-M. Liu, *Phys. Rev. Lett.* **108**, 080406 (2012).
- [66] W. Han, X.-F. Zhang, D.-S. Wang, H.-F. Jiang, W. Zhang, and S.-G. Zhang, *Phys. Rev. Lett.* **121**, 030404 (2018).
- [67] W. Zheng, Z.-Q. Yu, X. Cui, and H. Zhai, *J. Phys. B: At. Mol. Opt. Phys.* **46**, 134007 (2013).
- [68] J.-R. Li, W. G. Tobias, K. Matsuda, C. Miller, G. Valtolina, L. De Marco, R. R. Wang, L. Lassablière, G. Quéméner, J. L. Bohn *et al.*, *Nat. Phys.* **17**, 1144 (2021).